J. Eur. Opt. Society-Rapid Publ. 2026, **22**, 50
© The Author(s), published by EDP Sciences, 2026
https://doi.org/10.1051/jeos/2026034
Available online at: https://jeos.edpsciences.org

EOSAM 2025
Guest editors: Omar El Gawhary, Stefan Witte, Ignacio Moreno

Journal of the European Optical Society-Rapid Publications

RESEARCH ARTICLE OPEN ACCESS

Visualization of wavefront aberrations by Zernike polynomials

Stephan Reichelt*

Institute of Applied Optics (ITO), University of Stuttgart, Pfaffenwaldring 9, 70569 Stuttgart, Germany

Received 28 January 2026 / Accepted 31 March 2026

Abstract. Zernike aberration coefficients are typically presented in tabular form or as simple bar graphs, making it difficult to intuitively interpret their meaning and relate them to the specific aberration term. In this work, we present intuitive and rapidly interpretable visual representations of Zernike aberration terms that highlight the magnitude and orientation of their dominant contributions. Depending on the aberration order, we recommend different graphical formats – such as bubble plots and heatmaps – for visualizing low-order and mid-spatial frequency Zernike terms. These graphical representations are particularly valuable when quick visual feedback on individual aberration terms is needed, such as during aberration compensator adjustment, real-time wavefront visualization of dynamic processes, or optical alignment procedures. They can also enhance the clarity and interpretability of inspection reports or measurement certificates. Furthermore, an alternative definition of the azimuthal orientation of Zernike terms with $m \neq 0$ is proposed, enabling a more effective analysis of the shape and bending of spoke-shaped aberrations.

Keywords: Zernike polynomials, Visualization, Wavefront analysis, Wavefront aberrations, Optical testing.

1 Introduction

Polynomial sets such as Zernike polynomials [1–4] are widely used in various applications to approximate optical aberrations in a compact and sufficiently accurate manner. For example, in precision optical manufacturing, Zernike polynomials are used to characterize and approximate surface figure errors of optical components (e.g., lenses, flats) or wavefront aberrations of optical systems measured by interferometers or wavefront sensors. Freeform surfaces, which can also be described by Zernike polynomials, play an important role in optical design. In addition, Zernike polynomials are typically used in adaptive optics to compensate for dynamic aberrations, such as those caused by atmospheric turbulence.

The present work is motivated by the aim of providing a representation of Zernike approximation results that is as simple and intuitive as possible. Conventional formats such as tabular listings or bar plot visualizations, while widely used, often fail to adequately convey structural relationships and limit the direct interpretability of the underlying wavefront or surface characteristics. For users working with Zernike polynomial representations in optical design, metrology, or ophthalmology, the interpretation of coefficient sets can be non-trivial, particularly in the presence of multiple interacting modes or when spatial patterns must be inferred indirectly. This can make it difficult to extract relevant insights efficiently, even for experienced practitioners. To address this, the present work introduces a novel representation that is specifically designed to make structurally relevant features more directly accessible, thereby facilitating interpretation and supporting more effective analysis of Zernike-based wavefront or surface descriptions.

2 Definition of Zernike polynomials

Figure 1 illustrates the first 15 Zernike polynomials, arranged in a pyramid up to the 4th order.

Zernike polynomials are expressed either in Cartesian (x, y) or conveniently in polar coordinates (r, θ). They are defined within the unit circle, where r is the normalized radial distance from the origin, and θ is the angle from the x axis (common right-handed coordinate system). Apart from a preceding normalization factor N_n^m, Zernike polynomials are the product of a radial polynomial $R_n^m(r)$ and an azimuthal function $M_m(\theta)$

$$Z_n^m(r, \theta) = N_n^m \cdot R_n^m(r) \cdot M_m(\theta), \tag{1}$$

where n is the degree of the polynomial and m is the azimuthal dependence parameter [2, 5]. The azimuthal order m is an integer $(m \in \mathbb{Z})$, whereas the polynomial degree or radial order n is a non-negative integer $(n \in \mathbb{N}_0)$. For a particular Zernike polynomial Z_n^m, the integral values n and m are either both even or both odd. The double-indexing scheme, in which n denotes the highest power of the

* Corresponding author: reichelt@ito.uni-stuttgart.de

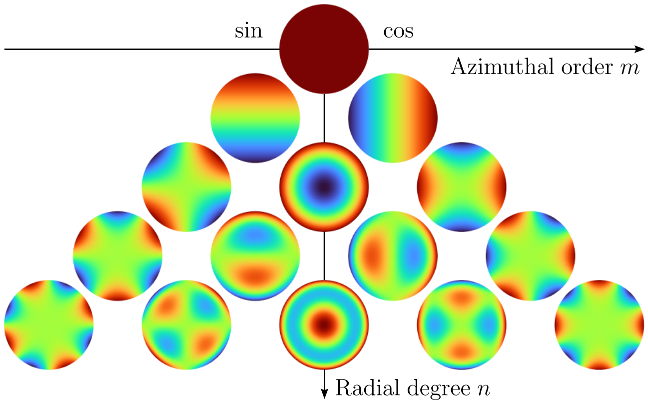

Fig. 1. Pyramid representation of the non-normalized Zernike polynomials Z_n^m up to the 4th order.

radial polynomial and m the azimuthal order, is essential for unambiguously describing the Zernike polynomials.

The radial polynomials $R_n^m(r)$ are explicitly defined by

$$R_n^m(r) = \sum_{s=0}^{\frac{n-|m|}{2}} \frac{(-1)^s (n-s)!}{s!\left(\frac{n+m}{2}-s\right)!\left(\frac{n-m}{2}-s\right)!} r^{n-2s}, \tag{2}$$

whereas the azimuthal function $M_m(\theta)$ is given by[1]

$$M_m(\theta) = \begin{cases} -\sin(m\theta) & \text{for } m < 0 \\ \cos(m\theta) & \text{for } m \geq 0 \end{cases}. \tag{3}$$

Optionally, a normalization factor N_n^m may be applied, defined as

$$N_n^m = \begin{cases} 1 & \text{for no normalization} \\ \sqrt{(2-\delta_{m0})(n+1)} & \text{for RMS normalization} \end{cases} \tag{4}$$

where δ_{m0} is the Kronecker delta function.[2] If the normalization factor N_n^m is set to 1, the Zernike polynomials are referred to as non-normalized, implying that either their maximum is 1 or that their maximum and minimum are ± 1, respectively. In contrast, for RMS-normalized polynomials, the normalization factor is defined such that the root-mean-square (RMS) value of each polynomial is 1. This ensures that, when a polynomial fit is applied to a data set, the absolute value $|c_n^m|$ of the fitted Zernike coefficients directly represent the RMS values of the associated aberration terms. For numerical reasons, it is advantageous to apply the RMS normalization not to the Zernike polynomials themselves, but to the coefficients obtained from the fit.

Note that each Zernike polynomial pair, Z_n^m and Z_n^{-m} (for $m \neq 0$), has the same normalization factor $N_n^m = N_n^{-m}$ as well as the same radial polynomial $R_n^m(r) = R_n^{-m}(r)$.

[1] Note that the sine function is an odd function where $\sin(-x) = -\sin(x)$. For $m < 0$, the negative sign of the sine function is necessary for a correct notation.
[2] Kronecker delta is defined as $\delta_{m0} = \begin{cases} 1 & \text{for } m = 0 \\ 0 & \text{for } m \neq 0 \end{cases}$.

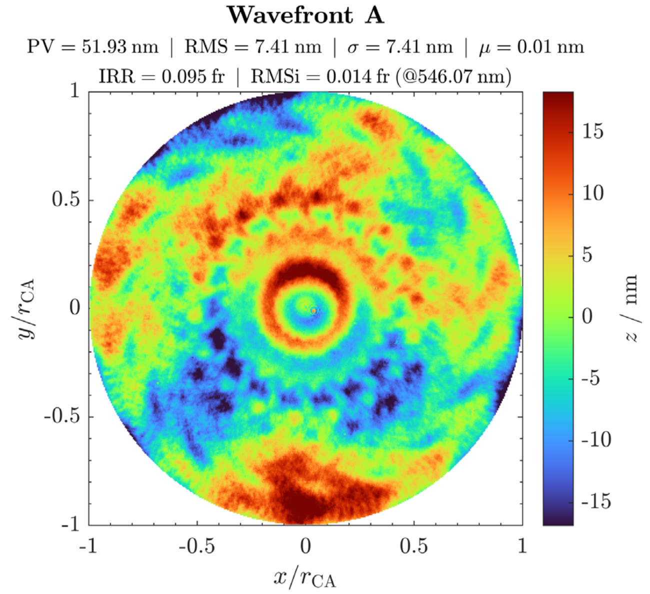

Fig. 2. Sample wavefront A: measurement data of a lens surface.

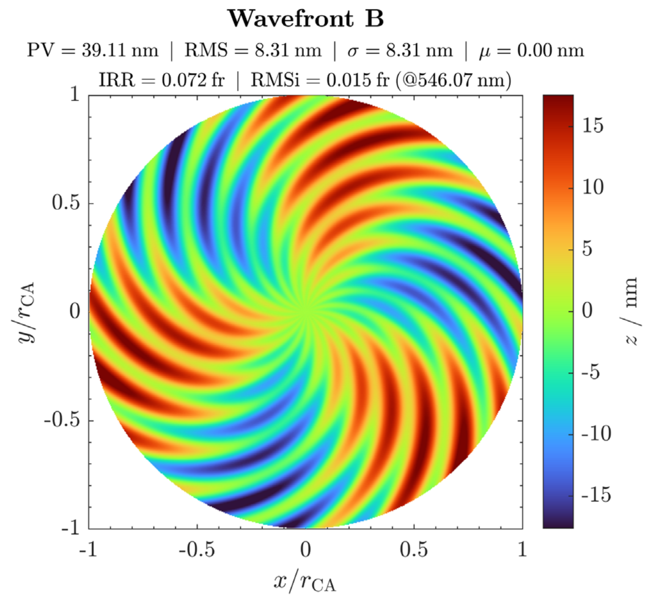

Fig. 3. Sample wavefront B: synthetic aberration data.

3 Sample wavefront data

Two representative wavefronts are employed to illustrate the visualization methods discussed in this paper. Wavefront A (Fig. 2) corresponds to the measured aberrations of a lens surface, containing both low- and mid-spatial frequency contributions, while wavefront B (Fig. 3) is synthetically generated to highlight the orientation of individual azimuthal orders.

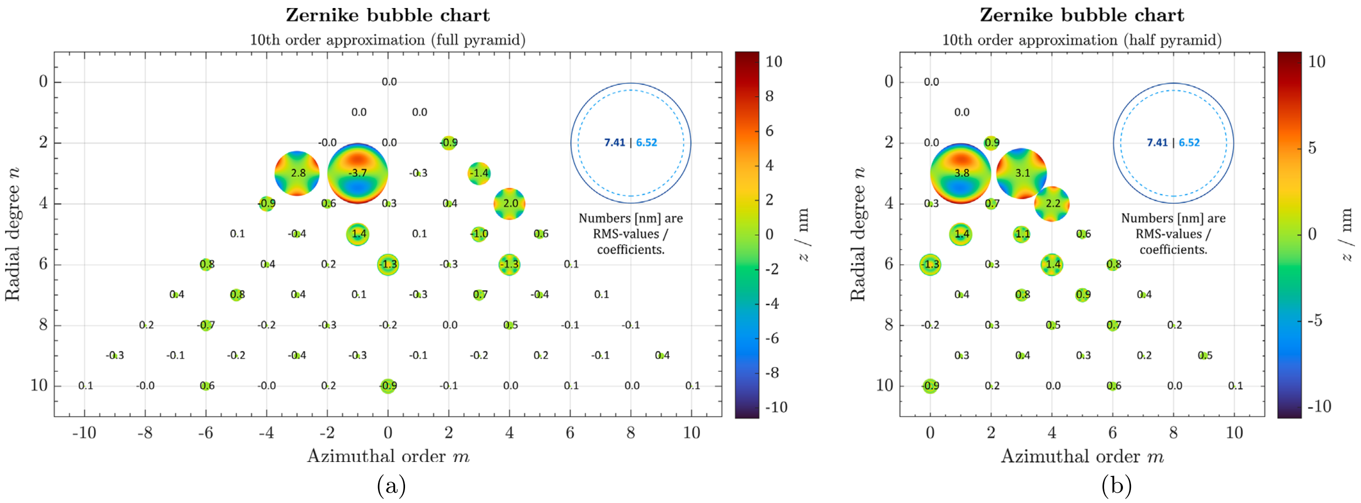

Fig. 4. Bubble chart plots of low-order Zernike aberration coefficients in full-pyramid representation (a) and in half-pyramid representation (b). The area of the depicted aberration terms (bubble size) is proportional to the magnitude of its RMS-normalized Zernike coefficient c_n^m. The blue circles on the upper right represent the areas of the total RMS-deviation of the wavefront error (dark blue) and its fitted RMS-deviation by the shown low-order aberrations fit of a 10th order polynomial (light blue). The numbers within the pyramid represent the RMS-normalized Zernike coefficients [nm], whereas the numbers in the blue reference circles (upper right corner) are the RMS-values [nm] of the original wavefront and its fitted 10th-order counterpart. Primary coma and trefoil are the main aberration terms.

4 Representing low-order Zernike aberrations

Often, the coefficients resulting from a least-squares Zernike fit are presented in tabular form or as simple bar graphs using a single-indexing scheme. However, Zernike polynomials depend on two integer parameters, n and m, which makes any single-indexing scheme arbitrary. This makes it difficult to interpret their meaning and relate them to the specific aberration term, especially since different single-index ordering schemes are in use, such as ANSI/ISO 24157, Born/Wolf, Standard, or Fringe.

Evans et al. [6] proposed a graphical representation, showing the magnitude of the various Zernike orders in dependence of the azimuthal order m and the degree n of the radial polynomial, a method that was adopted by the author years ago for plotting the aberration coefficients as two-dimensional bar plots, e.g. in [7].

Inspired by this, an even more intuitive way for representing low-order Zernike aberration coefficients is proposed here. It makes use of the Zernike pyramid and the fact, that the RMS-normalized Zernike coefficients are uncorrelated to each other. Hence, the root-sum-of-squares (rss) level of individual RMS-normalized Zernike coefficients c_n^m yields the total RMS-value of the aberration

$$\mathrm{RMS_{total}} = \sqrt{\sum_{i=1}^{\infty} \mathrm{RMS}_i^2} = \sqrt{\sum_{i=1}^{\infty} \left(c_n^m\right)_i^2}. \qquad (5)$$

The basic idea is just use a bubble plot depiction of the Zernike pyramid and scale the size of each individual bubble (or individual Zernike polynomial) with the magnitude of the RMS-normalized Zernike coefficient c_n^m. There is a physical meaning in this scaling as the sum of all individual bubble areas corresponds to the total RMS-value. By way of example this is shown in Figure 4a for an X/Y representation of the full Zernike pyramid.

Here, the total RMS deviation of sample wavefront A having 7.41 nm is taken as the reference area (area $\propto \mathrm{RMS}^2_{\mathrm{total}} \propto r^2_{\mathrm{total}}$, cf. dark blue circle in the upper right corner). The individual radii scale then with $\left|c_n^m\right|_i/\mathrm{RMS_{total}}$, i.e. the total area of all shown bubbles (10th order fit with 66 polynomials) therefore corresponds to the light blue dotted area $\propto \mathrm{RMS}^2_{10\mathrm{th}} = (6.52\,\mathrm{nm})^2$. It can be easily seen in Figure 4a that primary Y–coma and primary Y–trefoil are the main aberration contributors. An advantage of the full pyramid or X/Y representation is that the signs of the Zernike coefficients c_n^m are preserved, either through the positions of the maxima and minima of the individual Zernike terms or through additional numerical annotation.

Another, even more convenient depiction is a Mag/Angle representation utilizing only half of the Zernike pyramid, see Figure 4b. The magnitude of the paired X/Y coefficients is given by

$$|c_n^m| = \sqrt{\left(c_n^{-m}\right)^2 + \left(c_n^{+m}\right)^2}, \qquad (6)$$

whereas the angular orientation results just from adding up $\left(c_n^{-m} Z_n^{-m} + c_n^{+m} Z_n^{+m}\right)$ pairwise. Magnitude and orientation can be then interpreted intuitively.

Note that in Figure 4, the terms piston, tilt, and defocus have been set to zero intentionally, since they describe alignment parameters rather than intrinsic surface or wavefront aberrations.

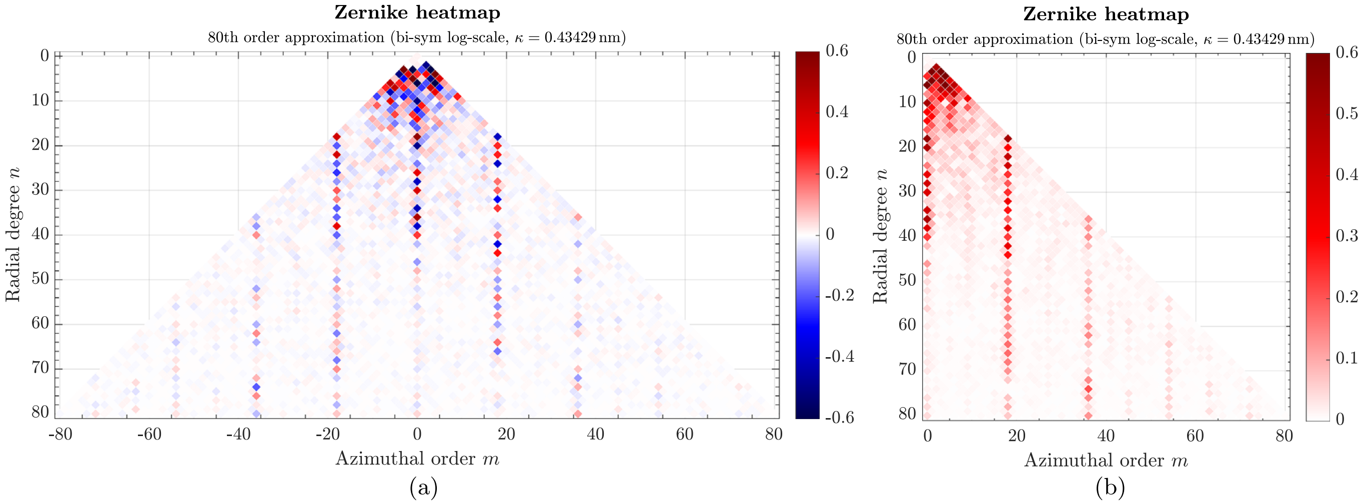

Fig. 5. Heatmaps of Zernike aberration coefficients for a 80th-order approximation in full-pyramid representation (a) and in half-pyramid representation (b). To emphasize coefficients with small magnitudes, the coefficients are displayed on a bi-symmetric logarithmic scale [8]. In the full-pyramid representation, the signs of the coefficients are preserved, whereas in the half-pyramid representation, the magnitudes of the respective coefficient pairs are shown.

5 Representing mid- and high-spatial frequency Zernike terms

Whereas the Zernike pyramid representation with scaled bubbles is adequate for visualizing polynomial degrees up to the 10th or 12th order, it becomes impractical for high-order fits. Zernike coefficient maps (also called Zernike spectra) are ideally suited for this purpose.

Figure 5 presents heatmaps of Zernike aberration coefficients obtained from a 80th-order fit of sample wavefront A. To emphasize coefficients with small magnitudes, the data are displayed using a bi-symmetric logarithmic scale [8]. The scaling constant of the bi-symmetric transfer function, which controls the slope near the origin, was set here to $\kappa = 1/\ln(10)$ nm.

Note that the heatmaps are not displayed as a conventional pixel grid, but instead as a square tiling rotated by 45° and rendered using patches. This representation avoids gaps in the spectrum and ensures that the pyramid is fully filled. Alternative spectral representations [9, 10] employ a modified radial index n_F for the same purpose, namely to circumvent such gaps. The representation presented here simultaneously provides a fully filled pyramid while preserving the conventional ordering of the radial polynomial degree n along the ordinate.

The log-based representation clearly reveals characteristic azimuthal orders with $m = 18$ and their higher harmonics ($m = 36,\ 54,\ 72$) in the wavefront. The heatmaps therefore reveal specific mid-spatial-frequency errors, such as ripple and spoke-like structures. Rotationally variant irregularities, or spoke-shaped aberrations, represent a specific form of surface undulations characterized by regular azimuthal orders extending toward the origin of the wavefront map. Such azimuthal waviness is typically introduced by manufacturing processes involving rotational motion about the workpiece center. Examples include precision contour grinding of lenses, where chatter marks may arise from ring tools, as well as diamond turning or direct laser beam writing using air-bearing spindles, where slight imbalances can cause run-out errors.

6 Azimuthal orientation

The angular or azimuthal orientation refers to the angle with respect to the positive x-axis at which the aberration occurs. For example, combining equal positive tilts in the x- and y-directions produces a resultant tilt oriented at $+45°$. For a tilt, the direction of the aberration is unambiguous when referenced to its maximum. However, once the radial polynomial contains more than one term, local maxima or minima arise along the radial profile. How, for example, should the orientation of primary coma (cf. Fig. 6, center) be specified? Two approaches can be considered. One may, for instance, refer to the maximum value at the edge of the aperture, i.e. at $r = 1$ (previous definition). Alternatively, one may refer to the first local maximum in radial direction, which for primary coma occurs at the radius $r = \sqrt{2/3} \approx 0.471$ (proposed definition). These two variants are discussed in more detail in the following.

In Evans et al. [6] an equation and procedure to determine the first peak in *angular* direction at the edge of the aperture (i.e. at radius $r = 1$) is derived, which further simplifies with the atan2-function to

$$\theta_0^{\mathrm{lp}} = \frac{1}{m}\,\mathrm{atan2}\big(c_n^{-m}, c_n^{m}\big), \tag{7}$$

where $m \in \mathbb{N}$. This variant is referred to here as the previous definition. The angular offset angle is denoted hereafter by the superscript “lp” which stands for “last peak in *radial* direction”. As can be seen from Figure 1, for all Zernike polynomials with a cosine azimuthal dependence ($m > 0$, right

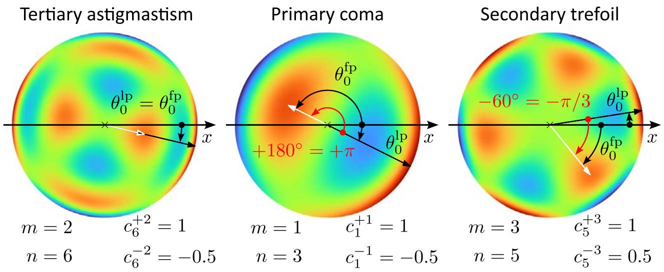

Fig. 6. Comparison of the definitions for azimuthal orientation of $\pm m$-paired Zernike polynomials. The angular orientation of the Zernike polynomials $Z_n^{\pm m}$ is illustrated for different choices of θ_0 (black arrow: common definition θ_0^{lp}; white arrow: proposed new definition θ_0^{fp}). Left: tertiary astigmatism $Z_6^{\pm 2}$ with peaks at same azimuthal orientation. Middle: primary coma $Z_3^{\pm 1}$, where $\pi = 180°$ has to be added. Right: secondary trefoil $Z_5^{\pm 3}$, where $\pi/3 = 60°$ must be subtracted.

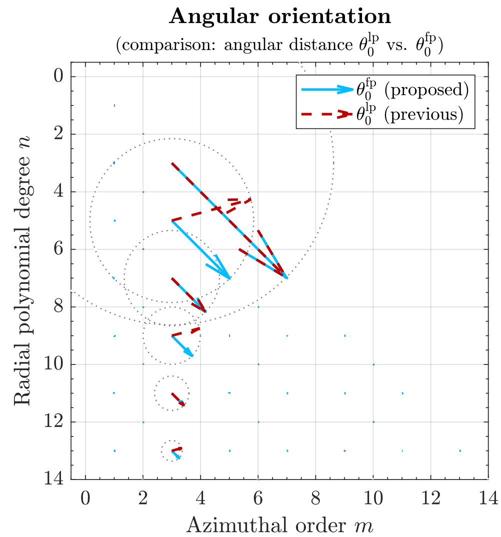

Fig. 7. Comparison of the two definitions for angular orientation. The vector length represents the magnitude of the Zernike coefficient $|c_n^m|$, and the angle represents its orientation.

side of pyramid) this last peak in radial direction at $r = 1$ is always located on the positive x-axis (at $x = 1$, $y = 0$).

Here, we define another angle θ_0^{fp} for the angular orientation, the one that points to the first local peak in the radial direction (proposed definition). The difference is illustrated in Figure 6.

If (n mod 4) = (m mod 4), then there is no difference in the definition. However, in all other cases (i.e., for every second diagonal wing pair of the Zernike pyramid, beginning with the primary coma pair), a special treatment is required. π/m must either be added or subtracted, depending on the signs of the coefficient pair, i.e.

$$\theta_0^{\mathrm{fp}} = \begin{cases} \theta_0^{\mathrm{lp}} & \text{if } (n \bmod 4) = (m \bmod 4) \\ \theta_0^{\mathrm{lp}} + \dfrac{\pi}{m} & \text{else if } (c_n^{-m} < 0) \vee (c_n^{-m} = 0 \wedge c_n^m > 0) \\ \theta_0^{\mathrm{lp}} - \dfrac{\pi}{m} & \text{else if } (c_n^{-m} > 0) \vee (c_n^{-m} = 0 \wedge c_n^m < 0) \end{cases} . \tag{8}$$

The three conditions can be combined into a compact formula suitable for implementation

$$\theta_0^{\mathrm{fp}} = \frac{1}{m}\operatorname{atan2}\left(c_n^{-m}, c_n^m\right) - \frac{\pi}{m}\{[(n-m) \bmod 4] \neq 0\}\operatorname{sign}\left[\operatorname{atan2}\left(c_n^{-m}, c_n^m\right)\right], \tag{9}$$

where the first term corresponds to equation (7), the bracketed factor $\{.\}$ represents a logical flag [0, 1] to distinguish the cases, and the sign-function determines whether π/m is added or subtracted.

The alternative definition of the azimuthal orientation of Zernike polynomials with $m \neq 0$ is motivated by the aim of enabling a more effective analysis of spoke-shaped aberrations. Consider the synthetically generated sample wavefront B (Fig. 3), which contains rotation-invariant aberration components only and is composed of spoke-shaped aberrations with azimuthal orders $m = 3$ (straight spokes) and $m = 18$ (bended spokes). The angular orientation of the straight, spoke-shaped trefoil in sample wavefront B is compared for both definitions in Figure 7. According to the previous definition (θ_0^{lp} as defined in equation (7), shown as red dashed arrows), the angle is rotated by π/m for every second occurrence of the polynomial degree n (i.e. $n = 5$, 9, 13, ...). In contrast, under the proposed definition (θ_0^{fp} according to equation (9), shown as light blue arrows), the angular orientation always points in the same direction (here $-45°$). This makes it possible to trace the radial progression of the spokes.

To analyze the bending or the shape of the spokes, representations other than the phasor plot in Figure 7 are more suitable. First, dominant azimuthal orders are identified by applying a threshold to the root-sum-square combination of the coefficients of a given order m. To plot the determined angles θ_0^{fp} as a function of radius, or to directly visualize their variation within the circular aperture, the radial coordinate of the first local maximum is required (cf. the endpoints of the white arrows in Fig. 6). This radius is determined numerically by searching for the first extremum of the corresponding radial polynomial R_n^m. The values are computed once and stored in a look-up table.

Note that the angle θ_0 in both equations (7) and (8) is confined to a circular sector spanning the arc $0 \pm \pi/m$. With increasing m, this minor sector becomes progressively smaller. As a consequence, owing to the arctan function, the evaluated angle θ_0 is wrapped modulo $2\pi/m$. To consistently trace the trajectory of a spoke from the aperture rim toward the coordinate origin, it can therefore be advantageous to unwrap the initial angle θ_0.

Figure 8 illustrates the proposed definition of the angle θ_0^{fp}, shown in (a) as a function of the radius and in (b) as a polar plot over the circular aperture.

The dominant azimuthal orders ($m = 3$ and $m = 18$) of sample wavefront B are presented, including both the wrapped angle (solid line with markers) and the unwrapped angle (dashed line without markers). Since, for $m = 3$, the

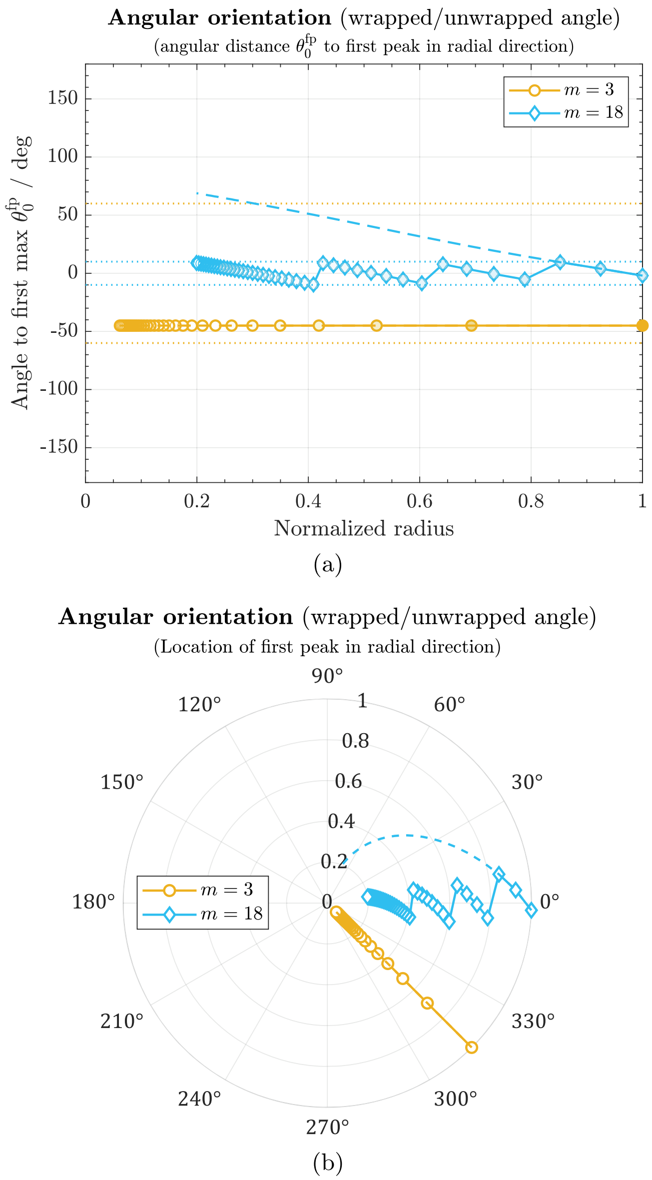

Fig. 8. Visualization of the proposed definition for azimuthal orientation. (a) Angle $\theta_0^{\mathrm{fp}}(r(n), m)$ over the radius where the first peak in radial direction occurs. (b) Polar plot of the same data.

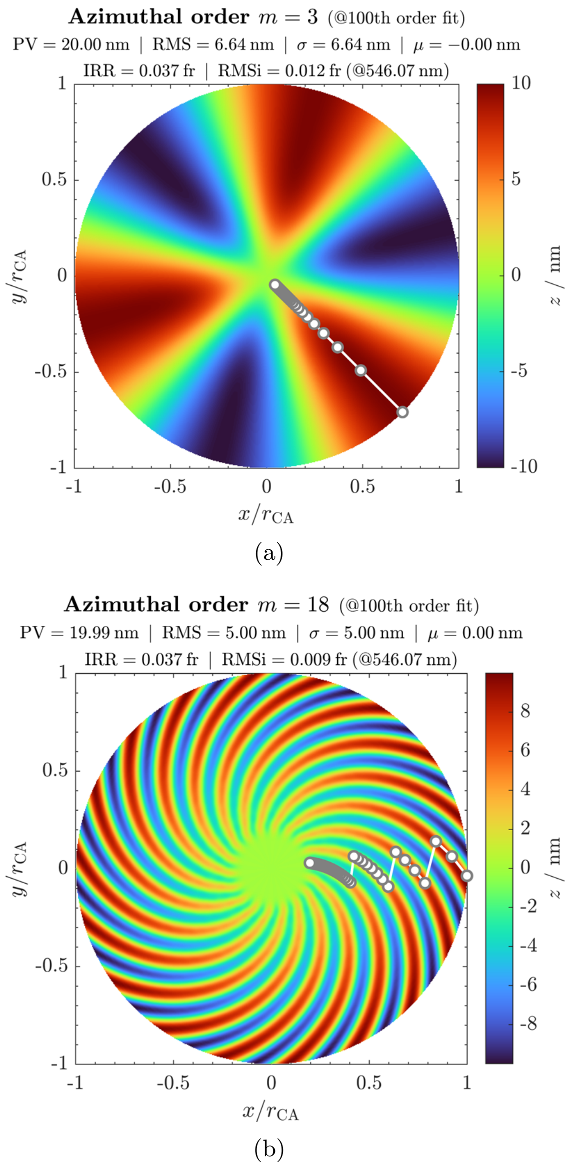

Fig. 9. Zernike-fit decomposition of the azimuthal orders of sample wavefront B, overlaid with the trajectory of the unwrapped angle θ_0^{fp}. A 100th-order Zernike fit was applied, with panel (a) showing the azimuthal order $m = 3$ and panel (b) showing $m = 18$.

wrapped angle never reaches the limit of uniqueness (indicated by the dotted line), the wrapped and unwrapped angles are here identical. The representation in Figure 8a reveals the radial dependence of the spoke bending. For $m = 3$, the bending is constant (straight spokes), whereas for $m = 18$ it exhibits a linear dependence on the radius. The polar plot in Figure 8b provides a convenient representation for tracing the trajectory of a single spoke of a given azimuthal order.

Finally, Figure 9 illustrates the fitted dominant orders (i.e., the sum of all Zernike terms with the same m), overlaid with the trajectory of the unwrapped angle θ_0^{fp}. Analyzing the shape and curvature of these spoke-like aberrations can therefore provide valuable insights into the underlying machine kinematics and support process optimization.

7 Summary

This paper presents a set of graphical visualization methods for results obtained from a Zernike approximation of wavefront aberrations or surface figure errors. These representations are intended to provide an intuitive visualization of the extensive information contained in the RMS-normalized Zernike coefficient vector. In particular, dominant characteristics are intended to be rapidly recognized and extracted.

Zernike bubble charts are well suited for representing low-order aberrations up to the 10th or 12th order. The area of each bubble is scaled according to the RMS value of the corresponding Zernike aberration, such that the relative scaling has a clear physical meaning. These bubble charts are particularly valuable when rapid visual feedback on individual aberration terms is required, for example during aberration compensator adjustment, real-time wavefront visualization of dynamic processes, or optical alignment procedures. In addition, they can improve the clarity and interpretability of inspection reports or measurement certificates for lenses and optical systems.

Zernike heatmaps, by contrast, are well suited for representing mid- and high-spatial-frequency errors. For this purpose, the magnitude of the RMS-normalized coefficients is displayed on a logarithmic scale in order to enhance the visibility of contributions with small amplitudes. Such heatmaps reveal characteristic manufacturing artifacts, such as spoke-like structures or ripple patterns.

Furthermore, this work introduces an alternative definition of the azimuthal orientation of Zernike terms for $m \neq 0$. This approach enables the identification of the shape and bending of spoke-like aberrations. For such specific analyses, other numerical methods, such as Fourier-based filtering or multi-angle averaging, may also be employed [11]. However, given the availability of convenient numerical methods for fitting wavefronts or aberrations to very high Zernike orders [12], these features can now be directly extracted from the Zernike coefficients themselves.

Funding

This research did not receive any specific funding.

Conflicts of interest

The author declares no conflicts of interest.

Data availability statement

The data that support the findings of this study are available from the corresponding author upon reasonable request. The MATLAB® code for visualizing Zernike coefficients (bubble charts, heatmaps) are publicly available on the MATLAB® File Exchange at the following URL: https://de.mathworks.com/matlabcentral/fileexchange/183649-zernike-visualization-heatmaps-and-bubble-plots.

Author contribution statement

This work was conducted and written solely by the author, who is fully responsible for all contributions and content.

References

1 Zernike F, Beugungstheorie des Schneidenverfahrens und seiner verbesserten Form, der Phasenkontrastmethode, *Physica* **1**(7), 689–704 (1934). https://doi.org/10.1016/S0031-8914(34)80259-5.

2 Malacara D (ed.), *Optical Shop Testing*, 2nd edn. (John Wiley & Sons, New York, 1992) https://doi.org/10.1002/9780470135976

3 Gross H, Dörband B, Müller H (eds.), *Handbook of Optical Systems, Volume 5: Metrology of Optical Components and Systems*, 1st edn. (Wiley-VCH, Weinheim, 2012) https://doi.org/10.1002/9783527699230.

4 Niu K, Tian C, Zernike polynomials and their applications, *J. Opt.* **24**(12), 123001 (2022). https://doi.org/10.1088/2040-8986/ac9c88.

5 Born M, Wolf E, *Principles of Optics*, 7th (expanded) edn. (Cambridge University Press, Cambridge, 1999).

6 Evans CJ, Parks RE, Sullivan PJ, Taylor JS, Visualization of surface figure by the use of Zernike polynomials, *Appl. Opt.* **34**(34), 7815–7819 (1995). https://doi.org/10.1364/AO.34.007815.

7 Reichelt S, Pruss C, Tiziani HJ, Absolute interferometric test of aspheres by use of twin computer-generated holograms, *Appl. Opt.* **42**(22), 4468–4479 (2003). https://doi.org/10.1364/AO.42.004468.

8 Webber JBW, A bi-symmetric log transformation for wide-range data, *Meas. Sci. Technol.* **24**(2), 027001 (2013). https://doi.org/10.1088/0957-0233/24/2/027001.

9 Forbes GW, Fitting freeform shapes with orthogonal bases, *Opt. Express* **21**(16), 19061–19081 (2013). https://doi.org/10.1364/OE.21.019061.

10 Hosseinimakarem Z, Davies AD, Evans CJ, Zernike polynomials for mid-spatial frequency representation on optical surfaces, *Proc. SPIE.* **9961**, 9961–18 (2016). https://doi.org/10.1117/12.2238514.

11 Reichelt S, Decomposition of non-rotationally symmetric wavefront aberrations into their azimuthal orders, in *Applied Optical Metrology III*, edited by E. Novak, J.D. Trolinger, (Proc. SPIE 11102, 2019), pp. 63–75. https://doi.org/10.1117/12.2526938.

12 Fan Y, Forbes GW, Rolland JP, Fast Zernike fitting of freeform surfaces using the Gauss-Legendre quadrature, *Opt. Express* **32**(11), 20011–20023 (2024). https://doi.org/10.1364/OE.498096.